新規光学素子への応用に向けたLa_2O_3–TiO_2系超高屈折率ガラスの研究開発

吉本幸平，髙須脩平，上田　基，井上博之，増野敦信

La_2O_3-TiO_2-based Ultra-high Refractive Index Glasses for Application as New Optical Elements

Kohei YOSHIMOTO, Shuhei TAKASU, Motoi UEDA, Hiroyuki INOUE and Atsunobu MASUNO

高屈折率ガラスは光学機器の小型化や収差性能等の向上に不可欠であるが，通常の光学ガラスでは着色や結晶化などの問題により屈折率が2.0以下に制限されている．La_2O_3–TiO_2 (LT) ガラスは無容器法による合成が可能であり，2.3を超える屈折率と可視域において良好な光透過性を示す有望な材料である．しかし，ガラスサイズの制約（数 mm 以下）が応用における大きな課題であった．本研究では，多成分系 LT ガラスを開発し，従来の二成分系 LT ガラスに比べて大幅なサイズ拡大（直径 25 mm）を実現した．これにより，精密な屈折率計測とモールドプレス成形によるレンズ試作が可能となった．さらに，高エネルギー X 線回折および第一原理分子動力学計算による構造解析の結果，カチオン－酸素多面体の高配位構造や稜・面共有が確認され，これらの構造的特徴が高イオン充填構造に寄与していることが示唆された．また，電子状態解析から，カチオン - 酸素間におけるイオン結合性と酸素の電子分極率との間に相関関係が確認された．上記結果は，LT 系ガラスの光学素材としての応用に向けたマイルストーンであるとともに，本ガラス系の物性発現機構の理解にも繋がる知見であると考えられる．

High-refractive-index glasses are essential for downsizing optical systems and improving their performance. La_2O_3-TiO_2 (LT) glasses are promising candidates owing to their remarkably high refractive indices (> 2.3) and good optical transmittance in the visible range. However, practical application of LT glasses is limited by their low glass-forming ability and small size of obtainable samples. This paper reports the development of new multicomponent LT-based glasses with enhanced glass stability, enabling the fabrication of significantly larger samples (up to 25 mm in diameter) compared to binary LT glass. Precise refractive index measurements showed values between 2.16 and 2.31. Despite their high refractive indices, these glasses maintained good transmittance in the visible region. Prototype lenses were successfully fabricated using a glass molding press, demonstrating their potential for practical applications. High-energy X-ray diffraction experiment and *ab initio* molecular dynamics simulations revealed a unique glass structure characterized by high cation-oxygen coordination numbers and a prevalence of edge- and face-sharing polyhedral connections, contributing to the high packing density. Electronic structure analysis indicated that the predominantly ionic nature of the cation-oxygen bonds increased electron polarizability of oxygen atoms. These findings provide a fundamental understanding of the ultra-high refractive index exhibited by LT-based glasses.

Key words ガラス，高屈折率，構造解析，第一原理計算，無容器法
glass, high refractive index, structural analysis, *ab initio* calculation, containerless processing

1 Introduction

Optical glasses are essential components in various optical applications, including digital imaging cameras, objective lenses of microscopes, endoscopes, and binoculars. High-refractive-index glass is particularly advantageous for miniaturizing optical systems owing to them requiring less curvature of the lens for achieving the same focal power compared to that made of low-refractive-index glass [1]. High-refractive-index lenses also contribute to high performance of optical systems such as reduced aberrations, high numerical aperture, and adequate working distances [2]. Recently, augmented reality and mixed reality glasses have emerged as next-generation smart devices, requiring high-refractive-index substrates for waveguides to achieve sufficient fields of view [3]. Consequently, the demand for high-refractive-index optical glass is increasing. However, developing practical optical glasses with refractive indices exceeding 2.0 is challenging owing to limitations in glass stability against crystallization and coloration [4].

The La_2O_3–TiO_2 (LT) system is a promising candidate to address these issues. Binary LT glasses can be synthesized using containerless processing without requiring typical network formers such as SiO_2, B_2O_3, P_2O_5, and GeO_2 [5]–[8]. LT glasses exhibit significantly high refractive indices (> 2.3) and relatively high optical transmittance in the visible range despite the high refractive index [6]. The glass-forming region of the binary LT system is reportedly narrow, ranging from 66.7 to 76.2 mol% TiO_2, and the resulting glass size is typically limited to 2–3 mm in diameter [7]. To develop LT-based glasses for practical applications as optical materials, enlarging glass sizes and precisely measuring the optical properties are necessary. This study aimed to develop new LT-based multicomponent glasses that enable larger glass sizes and precise determination of optical properties. Furthermore, the mechanisms underlying the unique optical properties of LT-based glasses were investigated by analyzing the glass structures and electronic states through diffraction experiment and molecular dynamics simulations.

2 Methods

2.1. Glass Synthesis

Six multicomponent LT-based glasses were prepared. High-purity La_2O_3, Y_2O_3, TiO_2, ZrO_2, Ta_2O_5, Al_2O_3, and SiO_2 were mixed in stoichiometric ratios. The oxide components of each composition and sample name, abbreviated according to their composition, are presented in Table 1. For each composition, the mixed powder was pressed into a cylindrical pellet at 20 MPa and air-sintered at 1200°C for 12 h. The sintered pellet was placed on the gas nozzle of a self-built aerodynamic levitation system and levitated using airflow. The levitated sample was heated using 100 W CO_2 lasers. Post-melting, the lasers were turned off, and the melt was allowed to cool naturally to room temperature to form a glass.

2.2. Measurements of Thermal and Optical Properties

The glass transition temperature (T_g) and crystallization onset temperature (T_x) were determined by differential thermal analysis in air at a heating rate of 10°C/min using a Thermo Plus EVO2 TG8121 thermal analyzer (Rigaku Co. Ltd., Tokyo, Japan). All glass samples were annealed at approximately their T_g to remove internal strain. Density was measured using an AccuPyc II 1340 gas pycnometer (Micromeritics Instrument Co., Norcross, USA) with an accuracy of ± 0.01 g/cm^3. Refractive index was measured using one of three methods, depending on the sample size: the prism coupling, V-block, or minimum deviation methods. Details of the measurement procedure by the prism coupling method are described in our previous work [9]. Measurements by the V-block method were performed using a Kalnew KPR-3000 precision refractometer (Shimadzu Corp., Kyoto, Japan) with an accuracy of $\pm 1 \times 10^{-5}$. The measurements by minimum deviation method were performed using an HR SpectroMaster UV-VIS-IR high-precision spectrorefractometer (Trioptics GmbH, Hamburg, Germany) with an accuracy of $\pm 1 \times 10^{-6}$. Optical transmittance spectra were acquired at 300–700 nm using a UH4150 UV-Vis-NIR spectrophotometer (Hitachi High-Tech Corp., Tokyo, Japan).

2.3. Diffraction Experiment

High-energy X-ray diffraction (HEXRD) experiment was conducted at the BL04B2 beamline of the SPring-8 synchrotron radiation facility [10] for LTZ using 113 keV X-rays. The total correlation function ($T^x(r)$) was then obtained by the Fourier transformation of the structure factors from 0.3 to 22 Å^{-1}.

2.4. Molecular Dynamics Simulations

Structural models of six LT-based glasses were constructed using *ab initio* molecular dynamics (AIMD) simulations based on density functional theory. Simulations were performed using hybrid Gaussian and plane wave method implemented in the QUICKSTEP module of the CP2K code [11]. Details of the AIMD simulations are shown in Nikon Research Report Vol. 3. The classical molecular dynamics (CMD) simulations with the LAMMPS code were used to create the initial configuration for AIMD simulations [12]. Each simulation model contained approximately 550 atoms. Multiwfn software package was used for post-processing and electronic structures, including calculations of electron populations, bond orders, and localized functions were analyzed [13], [14].

Table 1 Oxide components contained in LT-based multicomponent glasses

	Oxide components
LT	La_2O_3, TiO_2
LTZ	La_2O_3, TiO_2, ZrO_2
LTS	La_2O_3, TiO_2, SiO_2
LTZS	La_2O_3, TiO_2, ZrO_2, SiO_2
LTZTS	La_2O_3, TiO_2, ZrO_2, Ta_2O_5, SiO_2
LYTZAS	La_2O_3, Y_2O_3, TiO_2, ZrO_2, Al_2O_3, SiO_2

3 Results and Discussion

3.1. Thermal Properties

Table 2 presents the results of thermal analysis and density measurements. The temperature gap between T_x and T_g, denoted as ΔT (= T_x − T_g), is used as a measure of glass stability against crystallization [15]. The results indicate that both ZrO_2 and SiO_2 enhance the thermal stability of the glass, with LTZS (containing both ZrO_2 and SiO_2) exhibiting the highest ΔT among the fabricated samples. Therefore, we attempted to increase the size of the LT-based multicomponent glasses using a larger-diameter gas nozzle. Consequently, larger glass samples were successfully fabricated: approximately 10 mm in diameter for LTZ, 15 mm for LTS and LTZTS, and 25 mm for LTZS and LYTZAS. However, for the binary LT, glasses with diameter larger than 3 mm could not be obtained owing to crystallization. Figure 1 shows the photograph of LT and LTZS.

3.2. Optical Properties

Larger sample sizes enabled precise refractive-index measurements, which were previously challenging with the typical 2–3 mm diameter glasses obtained by containerless processing. The refractive indices of LT were measured using the prism coupling method; LTS and LTZTS were measured using the V-block method; and LTZ, LTZS, and LYTZAS were measured using the minimum deviation method. Figure 2 presents the refractive index (n_d) and the Abbe number (ν_d) of the LT-based glasses, comparing them with those of commercial optical glasses. The Abbe number was calculated from the refractive indices at the F (486.133 nm), d (587.562 nm), and C (656.273 nm) lines as follows:

$$\nu_d = \frac{n_d - 1}{n_F - n_C} \quad (1)$$

In Fig. 2, the LT-based glasses exhibit significantly higher refractive indices and relatively larger dispersion compared

Table 2 Thermal properties and densities of LT-based glasses

	T_g (°C)	T_x (°C)	ΔT (°C)	ρ (g/cm^3)
LT	800	862	62	4.91
LTZ	810	922	112	5.06
LTS	781	916	135	4.57
LTZS	794	973	179	4.88
LTZTS	793	966	173	5.11
LYTZAS	811	920	109	4.89

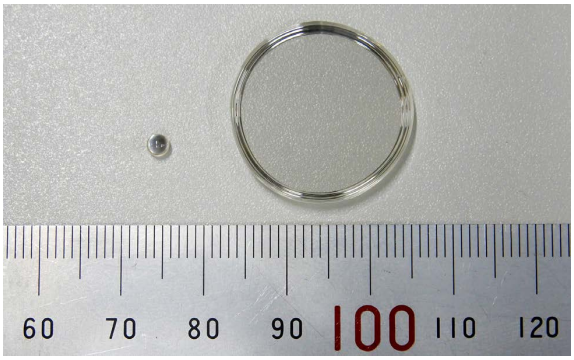

Fig. 1 Photograph of LT (left, 2.8 mm in diameter) and LTZS (right, 23 mm in diameter): LTZS is polished into disk (3 mm thickness) for the optical property measurement.

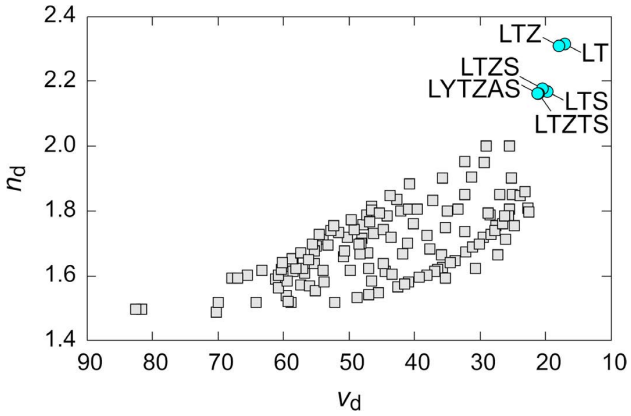

Fig. 2 Comparison of LT-based glasses (cyan circles) and commercial optical glasses (gray squares) in n_d vs. ν_d plot

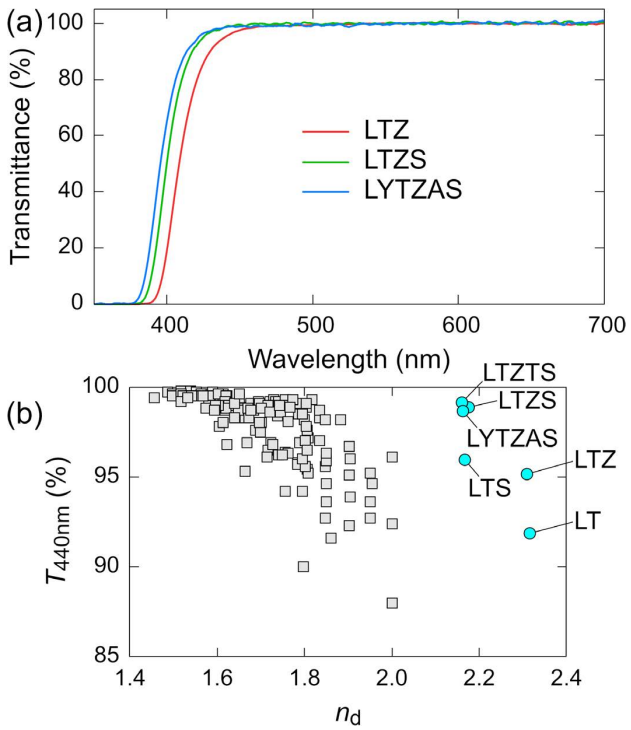

Fig. 3 (a) Internal transmittance spectra of LTZ, LTZS, and LYTZAS (10 mm thickness)
(b) Comparison of T_{440nm} and n_d for LT-based glasses (cyan circles) and commercial optical glasses (gray squares)

to the commercial optical glasses. LT and LTZ show particularly high refractive indices around 2.3, while the other SiO_2-containing compositions have refractive indices around 2.17.

The internal transmittance spectra of the LT-based glasses (10 mm thickness) are shown in Fig. 3(a). High transmittance is observed in the visible range, with a sharp absorption edge near 400 nm. Figure 3(b) shows the relationship between the internal transmittance at 440 nm (T_{440nm}, 10 mm thickness) and the refractive index (n_d) for both the LT-based glasses and commercial optical glasses. For both glass families, T_{440nm} tends to decrease with increasing n_d. However, the LT-based glasses maintain relatively high transmittance despite having significantly higher refractive indices than the commercial optical glasses.

3.3. Glass Molding Press

In this study, we developed multicomponent LT-based glasses with improved thermal stability, achieving glass sizes significantly larger than the typical 2–3 mm diameter obtained by containerless processing. These results motivated us to fabricate prototype lenses using a glass molding press in which glass preforms are reheated and molded into their final shape. The preform of LT-based glasses was placed between the molds and heated to a molding temperature above T_g of the sample. Once the molding temperature was reached, the upper mold was pressed onto the glass preform, giving it the shape of the mold. The molded sample was then released from the mold and polished to obtain the prototype lens. Using this method, a 25 mm diameter concave meniscus lens (Fig. 4(a)) and a 27 mm diameter biconvex lens (Fig. 4(b)) were fabricated from 20 mm diameter LYTZAS preforms. Furthermore, a 41 mm diameter, 1 mm thick wafer-shaped sample (Fig. 4(c)) was fabricated from a 22 mm diameter LTZS preform. No cracks or crystallization were observed in the molded samples. These results are expected to significantly expand the application potential of ultra-high refractive index glasses produced by containerless processing.

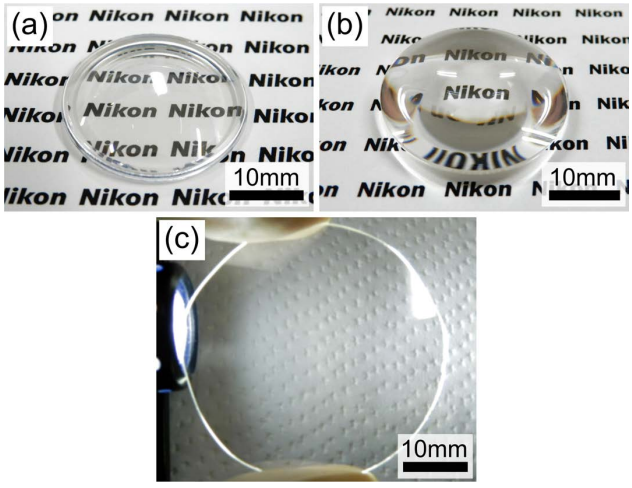

Fig. 4 Photographs of the prototype lenses of LT-based glasses fabricated using the glass molding test: (a) concave meniscus lens (LYTZAS, 25 mm in diameter), (b) biconvex lens (LYTZAS, 27 mm in diameter), and (c) wafer (LTZS, 41 mm in diameter).

3.4. Glass Structures

The X-ray weighted total correlation functions ($T^X(r)$s) for LTZ obtained from HEXRD experiments and AIMD are shown in Fig. 5(a). The AIMD-derived $T^X(r)$ agrees well with the experimental result, reproducing both the short-range order (~1–5 Å) and medium-range order (~5–10 Å) accurately. However, the mismatch at approximately 4 Å suggest that the M–M distance was reproduced slightly shorter in AIMD. The R_x factor, an agreement index [16] between the experimental and calculated $T^X(r)$s (calculated over the range of 1–10 Å), was 2.8%. Figure 5(b) shows the struc-

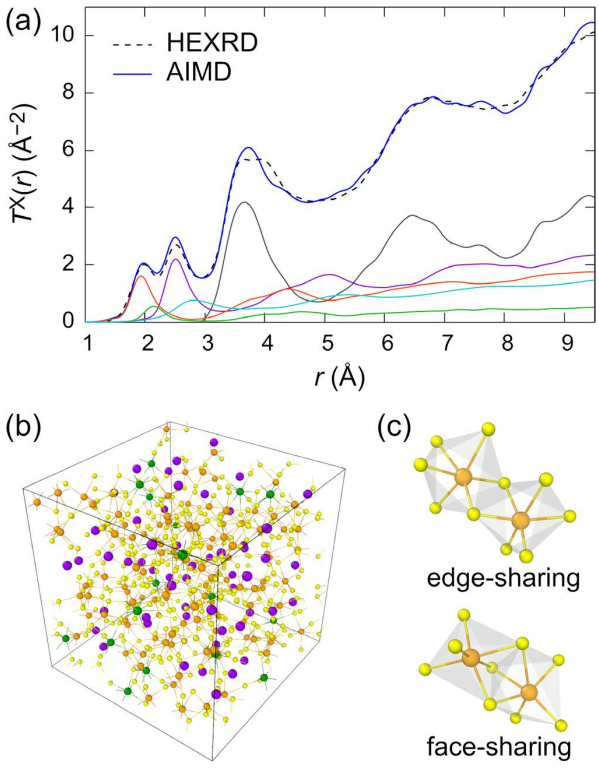

Fig. 5 (a) X-ray weighted total correlation functions, $T^X(r)$s, of LTZ obtained from HEXRD and AIMD simulations. Partial correlation functions for Ti–O (orange), La–O (violet), Zr–O (green), O–O (cyan), and M–M (gray) obtained from AIMD are also shown. (b) Snapshot of the LTZ structure obtained by AIMD simulation (c) Snapshot of edge- and face-sharing TiO_6–TiO_6 polyhedral linkages from the AIMD-derived structure
Atom colors: Ti (orange), Zr (green), La (violet), and O (yellow)

Table 3 Average M–O coordination numbers in LT-based glasses derived from AIMD

	N_{La-O}	N_{Y-O}	N_{Ti-O}	N_{Zr-O}	N_{Ta-O}	N_{Al-O}	N_{Si-O}
LT	8.97	–	5.67	–	–	–	–
LTZ	8.91	–	5.69	6.89	–	–	–
LTS	8.48	–	5.47	–	–	–	4.00
LTZS	8.83	–	5.68	7.06	–	–	4.08
LTZTS	8.74	–	5.58	6.94	6.11	–	4.15
LYTZAS	8.83	7.36	5.70	6.76	–	4.80	4.26

tural model of the LTZ obtained from AIMD simulation. The model suggests average M–O (M denotes the metal cation) bond lengths of 1.90 Å (Ti–O), 2.13 Å (Zr–O), and 2.49 Å (La–O) and average M–O coordination numbers of 5.69 (Ti–O), 6.89 (Zr–O), and 8.91 (La–O). A distinctive structural feature of LTZ is the large fraction of edge- and face-sharing connections between MO_n polyhedra (Fig. 5(c)). The connectivity between TiO_n polyhedra in LTZ was 69.8% corner-sharing, 28.9% edge-sharing, and 1.2% face-sharing, while the connectivity between LaO_n polyhedra was 35.7% corner-sharing, 48.7% edge-sharing, and 15.7% face-sharing. These structural features of high coordination numbers and prevalence of edge- and face-sharing polyhedral connectivity in LTZ do not follow the well-known Zachariasen's rules for glass formation [17].

Regarding the structural features of the LT-based glasses, Table 3 lists the average M–O coordination numbers derived from the AIMD simulations. Si, a typical network-former cation, exhibits 4-fold coordination with oxygen atoms. By contrast, transition metal cations (Ti, Zr, and Ta) show higher oxygen coordination numbers (approximately 6–7), and rare-earth cations (La and Y) have even higher coordination numbers (approximately 8–9 and 7, respectively). Figure 6 shows the average M–O coordination number (N_{M-O}) and the percentage of edge- and face-sharing MO_n–MO_n polyhedral linkages calculated from the AIMD models. The LT-based glasses in this study exhibit a positive correlation between the total fraction of edge- and face-sharing linkages and N_{M-O}. This suggests that the high proportion of edge- and face-sharing polyhedral connections in these glasses can be attributed to the high oxygen coordination numbers of the constituent rare-earth and transition metal oxides. Edge- and face-sharing polyhedral linkages reduce the inter-cation distances compared to corner-sharing, resulting in significantly high oxygen packing density in LT-based glasses [6], and consequently, contributing to the high refractive index.

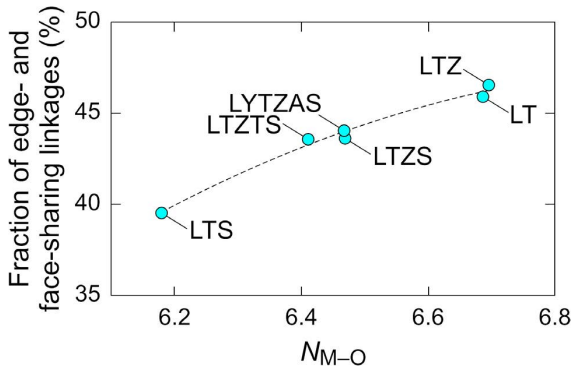

Fig. 6 Correlation between average coordination number (N_{M-O}) and the fraction of edge- and face-sharing polyhedral linkages in LT-based glasses (derived from AIMD simulations)
The dotted line is guide to the eye.

3.5. Electronic Structures

According to Mulliken population analysis [18], the net charge of atom A (ΔQ_A) is calculated by subtracting the gross atomic population (Q_A) from the nuclear charge (Z_A):

$$\Delta Q_A = Z_A - Q_A \tag{2}$$

Q_A is the sum of the net atomic population (Q_{AA}) and half of the total overlap population ($(1/2)\Sigma Q_{AB}$), where B represents an atom bonded to atom A:

$$Q_A = Q_{AA} + \frac{1}{2}\sum Q_{AB} \tag{3}$$

Q_{AA} and Q_{AB} are given by:

$$Q_{AA} = \sum_{\mu\in A}\sum_{\nu\in A}\sum_{i} n_i c_{\mu i} c_{\nu i} \int \chi_\mu(\mathbf{r})\chi_\nu(\mathbf{r})d\mathbf{r} \tag{4}$$

$$Q_{AB} = 2\sum_{\mu\in A}\sum_{\nu\in B}\sum_{i} n_i c_{\mu i} c_{\nu i} \int \chi_\mu(\mathbf{r})\chi_\nu(\mathbf{r})d\mathbf{r} \tag{5}$$

where $\chi_\mu(\mathbf{r})$ and $\chi_\nu(\mathbf{r})$ are the atomic orbitals; $c_{\mu i}$ and $c_{\nu i}$ are the contribution of $\chi_\mu(\mathbf{r})$ and $\chi_\nu(\mathbf{r})$ in the molecular orbital $\varphi_i(\mathbf{r})$; and n_i is the number of electrons in $\varphi_i(\mathbf{r})$. Figure 7 presents the results of population analysis based on above method for oxygen atoms in the LT-based glasses. The average electronic polarizability of oxygen atoms (α_O) was calculated using the procedure described in [6]. While the gross atomic population of oxygen (Q_O) shows minimal variation, the net atomic population (Q_{OO}) and the total overlap population (ΣQ_{OM}) exhibit significant changes with oxygen polarizability. The decrease in ΣQ_{OM} with increasing α_O suggests a decrease in covalent nature of O–M bonds. Furthermore, the increase in Q_{OO} implies an increase in the number of non-bonding electrons on oxygen atoms, which likely contributes to the increased oxygen polarizability. Table 4 lists the average bond orders of M–O pairs in each glass, calculated using the aforementioned Mulliken scheme

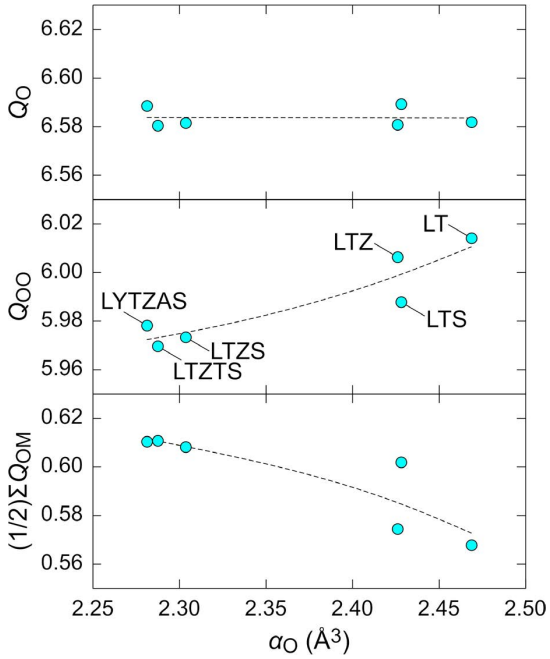

Fig. 7 Results of population analysis and electronic polarizability of oxygen atoms in LT-based glasses
Dotted lines are guides to the eye.

Table 4 Average bond orders of M–O pairs in LT-based glasses

	La–O	Y–O	Ti–O	Zr–O	Ta–O	Al–O	Si–O
LT	0.132	–	0.441	–	–	–	–
LTZ	0.132	–	0.435	0.393	–	–	–
LTS	0.145	–	0.445	–	–	–	0.873
LTZS	0.135	–	0.432	0.381	–	–	0.853
LTZTS	0.136	–	0.440	0.388	0.524	–	0.840
LYTZAS	0.135	0.241	0.431	0.395	–	0.409	0.821

(equivalent to Q_{MO} in Eq. (5)). Si–O bonds exhibit high values of bond order (> 0.8), indicating strong covalent character. By contrast, the transition metal and rare-earth cations, which are the primary components of the LT-based glasses, exhibit much lower values of bond order, indicating predominantly ionic bonds with oxygen atoms. These highly ionic characters increase the net atomic population of oxygen atoms (Q_{OO}), resulting in high electron polarizability of oxygen atoms.

Finally, the chemical bonding nature was visualized using the electron localization function (ELF) [19], as shown in Fig. 8. ELF is an indicator of electron localization in space [20]. In Fig. 8, the ELF localizes between Si and O atoms, indicating shared electron pairs and strong covalency of Si–O bonds. Meanwhile, the spherical distribution of ELF around oxygen atoms in Ti–O bonds suggests a more ionic bonding character.

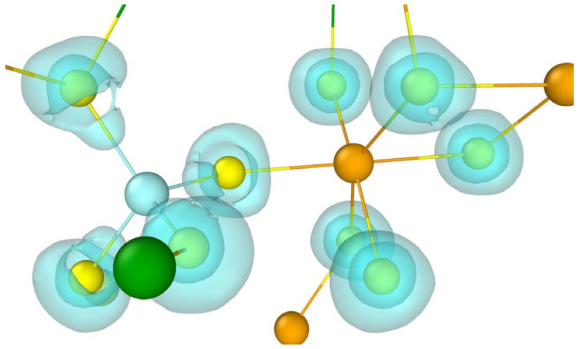

Fig. 8 ELF isosurface at level of 0.82 for SiO_4–TiO_6 fragment extracted from AIMD model of LTZS
Colors of atoms: Ti(orange), Zr (green), Si (cyan), and O (yellow)

4 Conclusion

This study successfully developed new multicomponent La_2O_3–TiO_2 (LT)-based glasses exhibiting enhanced thermal stability and significantly larger sizes compared to binary LT glasses. The incorporation of ZrO_2 and SiO_2 improved glass stability, enabling the fabrication of samples suitable for precise optical measurements and prototype lens production via glass molding press. These LT-based glasses exhibited exceptionally high refractive indices (n_d = 2.16–2.31) and good transmittance in the visible range, making them suitable candidates for a variety of optical applications. Structural analysis revealed a unique glass structure characterized by high coordination numbers and abundant edge- and face-sharing polyhedral linkages, possibly contributing to increased packing density. Notably, containerless processing allowed for achieving the glassy structure despite the presence of large fraction of edge- and face-sharing linkages. Furthermore, the predominantly ionic character of the cation–oxygen bonds resulted in increased oxygen polarizability, further enhancing the refractive index. This study demonstrated the potential of multicomponent LT-based glasses for practical applications requiring high-refractive-index materials. The findings indicate scope for future advancements in the miniaturization and performance enhancement of optical devices.

Acknowledgment. High-energy X-ray diffraction experiment was performed at beamline BL04B2 of SPring-8 under the approval of the Japan Synchrotron Radiation Research Institute (Proposal No. 2021A1297). This research utilized computational resources of the Oakforest-PACS supercomputer system provided by the Information Technology Center at the University of Tokyo. The authors thank all the members

at Advanced Technology Research & Development and Production Technology in Nikon Corp. for their support to this work.

References

[1] G. S. Jha, G. Seshadri, A. Mohan, and R. K. Khandal, "Sulfur containing optical plastics and its ophthalmic lenses applications," *e-Polym.,* vol. 8, no. 035, pp. 1–27, 2008.

[2] K. Watanabe and A. Nonaka, "Objective lens, optical system, and microscope," US. Patent 11782253B2, Oct. 2023.

[3] A. Kalinina and A. Putilin, "Wide-field-of-view augmented reality eyeglasses using curved wedge waveguide," in *Proceedings of SPIE*, vol. 11350, France, 2020, pp. 27–34.

[4] W. H. Dumbaugh, "Heavy metal oxide glasses containing Bi_2O_3," *Phys. Chem. Glasses,* vol. 27, no. 3, pp. 119–123, 1986.

[5] Y. Arai, K. Itoh, S. Kohara, and J. Yu, "Refractive index calculation using the structural properties of $La_4Ti_9O_{24}$ glass," *J. Appl. Phys*., vol. 103, 094905, 2008.

[6] H. Inoue, Y. Watanabe, A. Masuno, M. Kaneko, and J. Yu, "Effect of substituting Al_2O_3 and ZrO_2 on thermal and optical properties of high refractive index La_2O_3–TiO_2 glass system prepared by containerless processing," *Opt. Mater.,* vol. 33, no. 12, pp. 1853–1857, 2011.

[7] M. Kaneko, J. Yu, A. Masuno, H. Inoue, M. S. V. Kumar, O. Odawara, and S. Yoda, "Glass formation in $LaO_{3/2}$–TiO_2 binary system by containerless processing," *J. Am. Ceram. Soc*., vol. 95, no. 1, pp. 79–81, 2011.

[8] A. Masuno, Y. Watanabe, H. Inoue, Y. Arai, J. Yu, and M. Kaneko, "Glass-forming region and high refractive index of TiO_2-based glasses prepared by containerless processing," *Phys. Status Solidi C*, vol. 9, no. 12, pp. 2424–2427, 2012.

[9] K. Yoshimoto, A. Masuno, M. Ueda, H. Inoue, H. Yamamoto, and T. Kawashima, "Low phonon energies and wideband optical windows of La_2O_3-Ga_2O_3 glasses prepared using an aerodynamic levitation technique," *Sci. Rep*., vol. 7, 45600, 2017.

[10] S. Kohara, M. Itou, K. Suzuya, Y. Inamura, Y. Sakurai, Y. Ohishi, and M. Takata, "Structural studies of disordered materials using high-energy X-ray diffraction from ambient to extreme conditions," *J. Phys.: Condens. Matter,* vol. 19, 506101, 2007.

[11] J. VandeVondele, M. Krack, F. Mohamed, M. Parrinello, T. Chassaing, and J. Hutter, "Quickstep: Fast and accurate density functional calculations using a mixed Gaussian and plane waves approach," *Comput. Phys. Commun*., vol. 167, no. 2, pp. 103–128, 2005.

[12] S. Plimpton, "Fast parallel algorithms for short-range molecular dynamics," *J. Comput. Phys.,* vol. 117, no. 1, pp. 1–19, 1995.

[13] T. Lu and F. Chen, "Multiwfn: A multifunctional wavefunction analyzer," *J. Comput. Chem*., vol. 33, no. 5, pp. 580–592, 2012.

[14] T. Lu, "A comprehensive electron wavefunction analysis toolbox for chemists, Multiwfn," *J. Chem. Phys*., vol. 161, 082503, 2024.

[15] A. Dietzel, "Glasstruktur und Glaseigenschaften," *Glastech. Ber*., vol. 22, pp. 41–50, 1948.

[16] A. C. Wright, "Neutron scattering from vitreous silica. V. The structure of vitreous silica: What have we learned from 60 years of diffraction studies?," *J. Non-Cryst. Solids*, vol. 179, pp. 84–115, 1994.

[17] W. H. Zachariasen, "The atomic arrangement in glass," *J. Am. Chem. Soc*., vol. 54, no. 10, pp. 3841–3851, 1932.

[18] R. S. Mulliken, "Electronic population analysis on LCAO–MO molecular wave functions. I.," *J. Chem. Phys*., vol. 23, no. 10, pp. 1833–1840, 1955.

[19] T. Lu and F.-W. Chen, "Meaning and functional form of the electron localization function," *Acta Phys.-Chim. Sin*., vol. 27, no. 12, pp. 2786–2792, 2011.

[20] A. Savin, R. Nesper, S. Wengert, and T. F. Fässler, "ELF: The electron localization function," *Angew. Chem. Int. Ed. Engl*., vol. 36, no. 17, pp. 1808–1832, 1997.

吉本幸平　Kohei YOSHIMOTO
生産本部 技術統括部 光学素材部
Optical Material Department
Technology Sector
Production Technology

髙須脩平　Shuhei TAKASU
先進技術開発本部 材料・要素技術研究所
Materials & Advanced Research Laboratory
Advanced Technology Research & Development

上田　基　Motoi UEDA
先進技術開発本部
Advanced Technology Research & Development

井上博之　Hiroyuki INOUE
東京大学
The University of Tokyo

増野敦信　Atsunobu MASUNO
京都大学
Kyoto University